APPENDIX A

MACHINE LEARNING-ASSISTED ULTRAFAST FLASH SINTERING OF HIGH-PERFORMANCE AND FLEXIBLE SILVER-SELENIDE THERMOELECTRIC DEVICES

A.1 Flash sintering manufacturing and Bayesian optimization

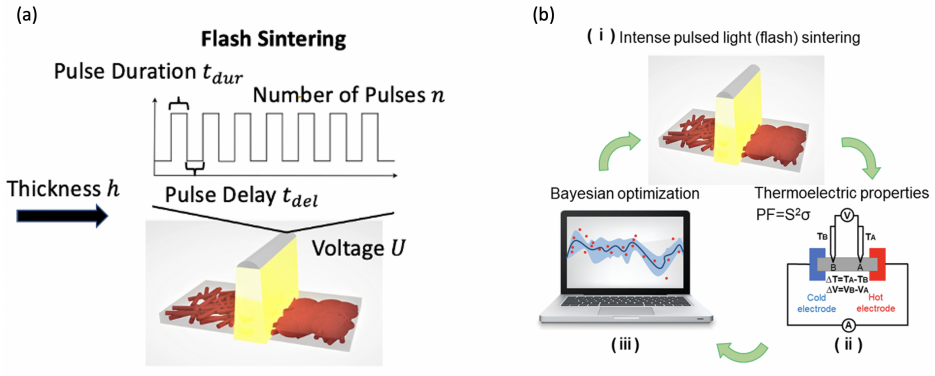

Figure A.1. (a) Schematic illustration of the flash sintering process, voltage, pulse duration, number of pulses, pulse delay, and thickness; (b) Schematic workflow of the machine learning-assisted flash sintering of silver-selenide TE films. (*i*) Intense pulsed light (flash) sintering. (*ii*) Thermoelectric properties measurement of the sintered film including the electrical conductivity, and the Seebeck coefficient. (*iii*) Bayesian optimization algorithm for the evaluation and suggestion of new sintering variables.

Figure A.1(b) depicts our machine learning-assisted workflow to find the optimum flash sintering variables for silver-selenide TE films fabricated using vacuum-assisted filtration technique. The aim of the framework is to find a set of variables including voltage, pulse duration, number of pulses, and pulse delay that yields the maximum power factor with a minimum number of experimental iterations. The workflow starts by flash sintering of silver-selenide films, then measuring the power factor of the films (Figure A.1(a)). The sintering variables and measured power factor is then used as an input for BO to predict the next set of variables to test.

TABLE A.1

FLASH SINTERING EXPERIMENTAL DATASET FOR HYPERPARAMETER TUNING EXPERIMENTS.

Sample #	Voltage (kV)	Pulse Time (ms)	Number of Pulses	Delay (ms)	Power Factor (kW/cm^2)
1	2.0	2.5	1	0	0.3
2	2.0	3.0	1	0	0.9
3	2.2	2.0	1	0	2.0
4	2.2	2.5	1	0	19.9
5	2.2	3.0	1	0	86.4
6	2.2	3.0	2	1000	118.6
7	2.2	3.0	3	1000	212.4
8	2.2	3.0	4	1000	315.8
9	2.2	3.0	5	1000	136.2
10	2.2	3.0	6	1000	184.9
11	2.2	3.0	8	1000	102.7
12	2.4	1.5	1	0	5.5
13	2.4	2.0	1	0	95.2
14	2.4	2.5	1	0	263.2
15	2.4	2.5	2	1000	410.1
16	2.4	2.5	3	1000	323.9
17	2.4	2.5	4	1000	160.9
18	2.4	2.5	5	1000	88.4

Continued on next page

TABLE A.1 (CONTINUED)

Sample #	Voltage (kV)	Pulse Time (ms)	Number of Pulses	Delay (ms)	Power Factor (kW/cm^2)
19	2.4	2.5	6	1000	29.6
20	2.4	2.5	8	1000	2.7
21	2.4	3.0	1	0	90.5
22	2.6	1.0	1	0	1.5
23	2.6	1.5	1	0	24.1
24	2.6	1.5	2	362	244.5
25	2.6	1.5	2	1000	90.4
26	2.6	1.5	3	1000	216.6
27	2.6	1.5	4	362	487.1
28	2.6	1.5	4	1000	320.4
29	2.6	1.5	5	362	726.0
30	2.6	1.5	5	1000	627.5
31	2.6	1.5	6	362	498.2
32	2.6	1.5	6	1000	325.2
33	2.6	1.5	8	362	465.1
34	2.6	1.5	8	1000	224.0
35	2.6	1.5	10	362	157.7
36	2.6	1.5	10	1000	38.0
37	2.8	1.0	1	0	28.5
38	2.8	1.5	1	0	55.1

TABLE A.2

DETAILS OF INTENSE PULSED LIGHT (FLASH) SINTERING CONDITIONS FOR EACH EXPERIMENT.

Sample	Thick. (μm)	Voltage (kV)	Pulse Time (ms)	Number Pulses	Pulse Del. (ms)	PF ($\mu W/mK^2$)
1	14.30	2.20	1.0	1	0	174.60
2	14.30	2.20	2.0	1	0	486.60
3	14.30	2.40	1.0	1	0	253.20
4	14.30	2.20	1.0	5	1000	322.90
5	14.30	2.40	1.0	5	1000	413.90
6	14.30	2.40	2.0	1	0	580.10
7	16.56	2.40	2.5	1	0	496.40
8	16.56	2.20	2.5	1	0	406.90
9	16.56	2.60	2.1	1	0	819.86
10	16.56	2.60	2.5	1	0	122.40
11	16.56	2.80	2.1	1	0	756.50
12	13.30	2.70	0.9	4	1500	886.47
13	13.30	2.70	0.9	10	1500	756.50
14	9.00	2.70	0.9	4	248	1037.54
15	9.00	2.70	0.9	10	248	1206.44
16	9.00	2.60	1.2	5	1000	966.59
17	9.00	2.60	1.2	10	1000	1126.32
18	9.00	2.60	1.2	5	298	1050.85
19	9.00	2.60	2.1	2	490	773.01

Continued on next page

TABLE A.2 (CONTINUED)

Sample	Thick. (μm)	Vol. (kV)	Pulse Time (ms)	Number Pulses	Pulse Del. (ms)	PF ($\mu W/mK^2$)
20	9.00	2.60	2.1	2	1000	467.07
21	9.00	2.60	1.7	2	404	1162.62
22	9.00	2.60	1.7	4	404	1259.78
23	2.35	2.20	0.5	1	0	288.70
24	2.35	2.20	1.0	1	0	901.90
25	2.35	2.20	2.0	1	0	1832.97
26	2.35	2.40	0.5	1	0	424.40
27	2.35	2.40	1.0	1	0	1411.70
28	2.35	2.40	2.0	1	0	1144.93
29	2.35	2.10	2.0	2	340	1719.45
30	2.35	2.15	1.9	2	340	1631.50
31	2.47	2.20	1.5	4	270	2123.32
32	2.45	2.30	1.5	4	293	2205.26
33	2.70	2.30	1.6	6	314	1453.98
34	2.70	2.20	2.2	2	413	933.71
35	2.70	2.30	1.7	10	335	1035.31
36	3.80	2.35	1.5	2	310	1259.18
37	3.80	2.20	1.5	7	270	1057.88

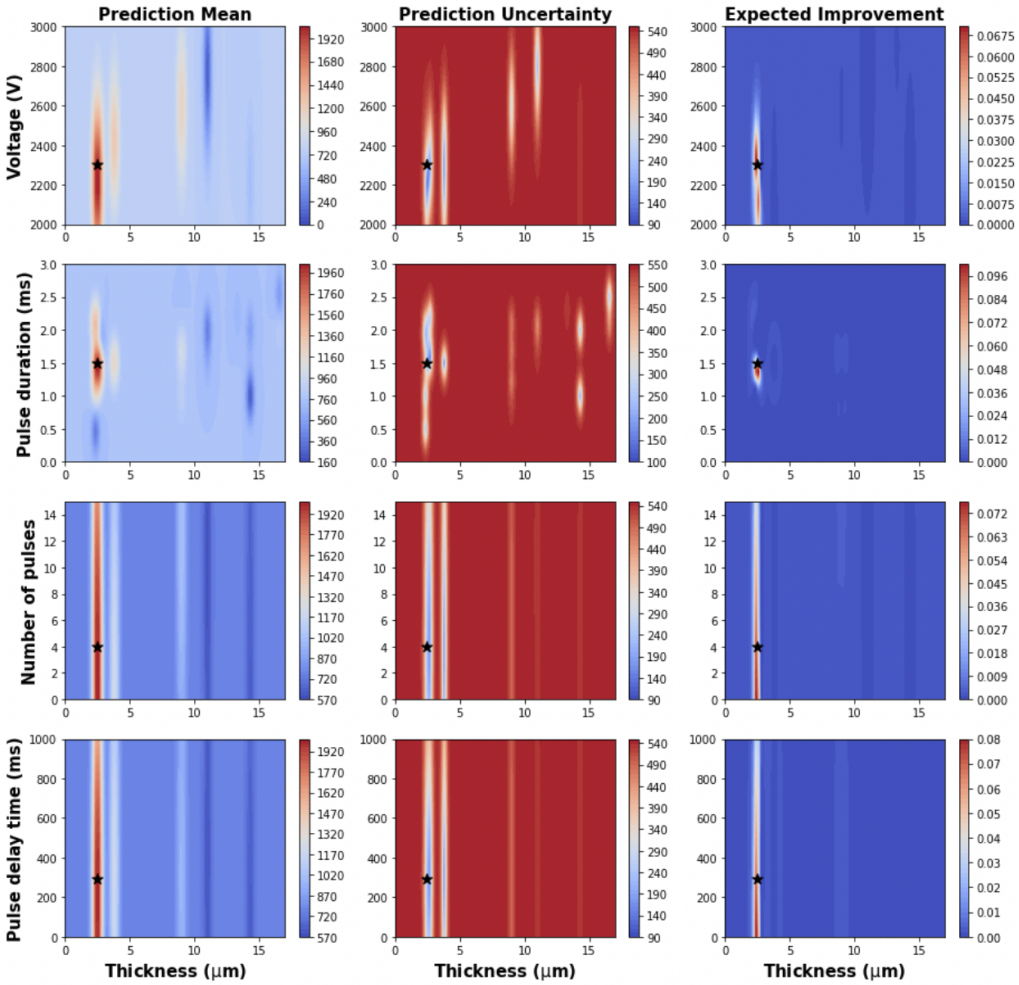

Figure A.2. Bayesian optimization prediction mean, uncertainty, and expected improvement from all data except the highest power factor.

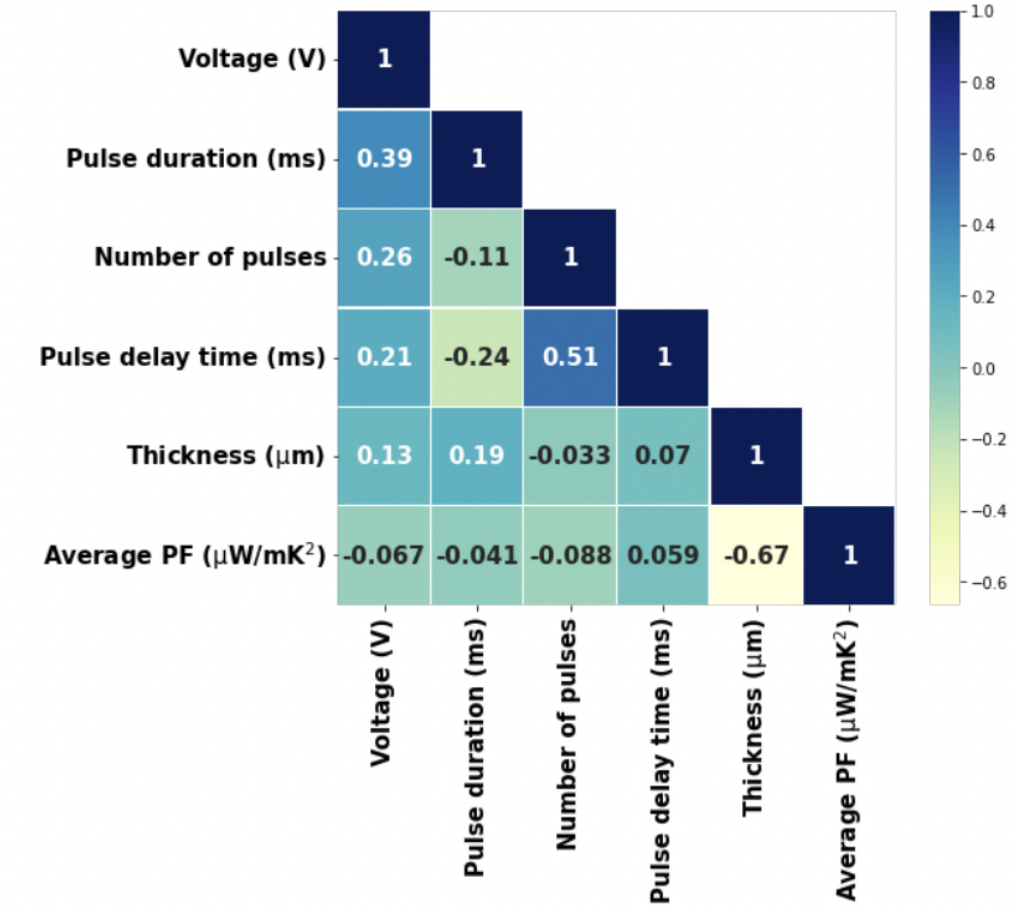

Figure A.3. Feature-feature correlation matrix of the top features.

APPENDIX B

BAYESIAN OPTIMIZATION OF LOW-TEMPERATURE NON-THERMAL PLASMA JET SINTERING OF NANOINKS

B.1 2-Probe measurement of ITO thin film's resistance

Electrical resistances of sintered ITO samples were measured with a 2-probe approach using an AMPROBE digital multimeter (CAT III). To minimize the influence caused by contact resistance, conductive silver paint (Spi, 05001-AB) was applied to the four corners of the square thin films, numbering 1 to 4, respectively, as illustrated in Figure B.1.

The measured resistance was determined as the average of measurements along the edges of the sample. For example, the resistance between points 1 and 2 was measured five times, and the average value was defined as R_{12}. Subsequently, the resistance between points 2 and 3 was measured five times, and the average value was defined as R_{23}. Similar measurements were conducted for R_{34} and R_{41}.

Two values were computed:

$$R = \frac{R_{12} + R_{34}}{2}, \quad R' = \frac{R_{41} + R_{23}}{2}, \tag{B.1}$$

and the difference between R and R' was less than 1.0%, indicating the ITO film was both coated and sintered uniformly. Given the negligible difference between R and R', the data reported here are only of R based on R_{12} and R_{34}.

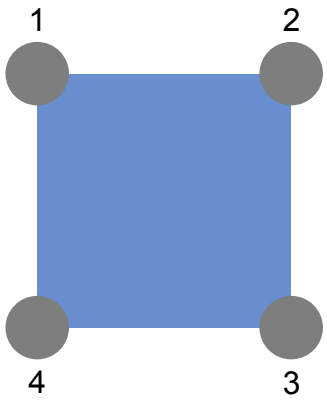

Figure B.1. Sketch of the contact pads for the 2-probe measurement of each ITO thin film's resistance. The blue square is the ITO thin film (3×3 mm^2), and the four gray circles are the contact pads of conductive silver paint (Spi, 05001-AB).

B.2 Initial nine plasma jet sintering experiments

Table B.1 summarizes the nine initial plasma jet sintering experimental conditions and the corresponding uncertainty for the measured electrical conductivity. These are the same experimental conditions in round 0 of BO, as shown in Tables B.3 and B.4. The uncertainty of the calculated electrical conductivity (δ_σ) was obtained using:

$$\delta_\sigma = \sqrt{\left(\frac{\partial \sigma}{\partial l}\delta_l\right)^2 + \left(\frac{\partial \sigma}{\partial R}\delta_R\right)^2}, \tag{B.2}$$

where δ_l is the uncertainty of the measured sintered ITO film's thickness and δ_R is the uncertainty of the measured 2-probe resistance of the sintered ITO film.

TABLE B.1

EXPERIMENTAL CONDITIONS AND UNCERTAINTIES FOR NINE INITIAL PLASMA JET SINTERING EXPERIMENTS.

Condition	n	t_{on} (min)	t_{off} (min)	Q (sccm)	U_a (kV)	f (kHz)	d (mm)	t_{active} (min)	t_{total} (min)	δ_σ (%)
1	2	8.0	8.0	500	5	30	2.5	16	32	8.20
2	1	6.0	6.0	1000	4	20	4.5	6	12	6.61
3	3	7.0	7.0	1500	4	20	3.5	21	42	4.55
4	1	16.0	16.0	500	4	60	3.5	16	32	9.28
5	2	10.0	10.0	1000	3	40	2.5	20	40	6.34
6	3	9.0	9.0	2000	3	30	3.5	27	54	7.97
7	2	9.0	9.0	500	4	20	4.5	18	36	6.80
8	4	6.0	6.0	500	5	40	3.5	24	48	7.75
9	4	7.0	7.0	1500	5	40	4.5	28	56	9.36

B.3 Machine learning modeling structure for plasma jet sintering optimization

Figure B.2 illustrates the modeling structure for optimizing plasma jet sintering, starting with a Gaussian Process Regression (GPR) model to maximize the SEI, followed by subsequent GPR models to maximize the electrical conductivity while ensuring a maximum substrate temperature below 50°C.

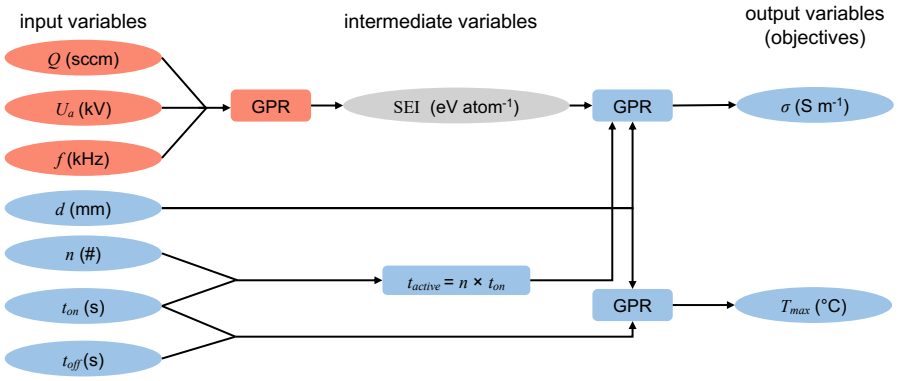

Figure B.2. Illustration of the model structure with variables (ovals), models (rectangles), and data flow (arrows). Jet flow rate (Q), applied voltage (U_a), and input frequency (f) directly determine the specific energy input (SEI), and their relationship is identified by a GPR model. Pulse-on time (t_{on}) and number of cycles (n) determine the active sintering time (t_{active}) for a plasma jet sintering experiment. A GPR model was developed based on SEI, d, and t_{active} for the optimization of the sample electrical conductivity; a separate GPR model was developed regarding d, t_{on}, and t_{off} for the optimization of peak substrate temperature.

B.4 Datasets

Table B.2 lists the 49 experiments comprising the 7-level full factorial for f and Q, and the measured U_{on} and U_{max} for Phase 1.

Table B.3 lists the nine rounds, each consisting of five to nine experiments for a total of 49, varying U_a, f, and Q in order to maximize SEI in Phase 2. Note that Round 0 was generated by Latin hypercube sampling of the entire space for the seven decision variables.

Table B.4 summarizes all five rounds of experiments with iterations based on Bayesian optimization recommendations to maximize the electrical conductivity of ITO films while controlling the peak substrate temperature as low as possible (Phase 3). The best plasma jet sintering result appeared in round 4 (highlighted in yellow), where the electrical conductivity of the sintered ITO sample was 7.272 S m^{-1} (81.4% compared with furnace sintering) with a peak substrate temperature of 46.5 °C and a total experimental time of one hour.

TABLE B.2

EXPERIMENTAL DATA FOR PLASMA JET SINTERING EXPERIMENTS.

Experiment	Q (sccm)	f (kHz)	U_{on} (kV)	U_{max} (kV)	δ_U (%)
1	100	20	2.9	6.1	3
2	400	20	2.8	6.2	3
3	700	20	2.7	6.0	3
4	1000	20	2.7	5.7	3
5	1300	20	2.6	5.7	3
6	1600	20	2.6	5.9	3

Continued on next page

TABLE B.2 (CONTINUED)

Experiment	Q (sccm)	f (kHz)	U_{on} (kV)	U_{max} (kV)	δ_U (%)
7	1900	20	2.6	5.9	3
8	100	30	2.6	7.3	3
9	400	30	2.5	6.1	3
10	700	30	2.6	5.7	3
11	1000	30	2.5	5.8	3
12	1300	30	2.5	5.6	3
13	1600	30	2.6	5.8	3
14	1900	30	2.3	5.7	3
15	100	40	2.5	7.2	3
16	400	40	2.5	5.7	3
17	700	40	2.3	5.6	3
18	1000	40	2.4	5.8	3
19	1300	40	2.3	5.7	3
20	1600	40	2.5	5.7	3
21	1900	40	2.3	5.6	3
22	100	50	2.5	8.7	3
23	400	50	2.3	5.5	3
24	700	50	2.2	5.5	3
25	1000	50	2.3	4.6	3
26	1300	50	2.3	4.6	3
27	1600	50	2.4	4.9	3
28	1900	50	2.5	4.4	3
29	100	60	2.6	8.1	3

Continued on next page

TABLE B.2 (CONTINUED)

Experiment	Q (sccm)	f (kHz)	U_{on} (kV)	U_{max} (kV)	δ_U (%)
30	400	60	2.4	5.1	3
31	700	60	2.3	4.5	3
32	1000	60	2.3	4.4	3
33	1300	60	2.2	4.4	3
34	1600	60	2.3	4.6	3
35	1900	60	2.3	4.3	3
36	100	70	2.5	7.6	3
37	400	70	2.3	4.5	3
38	700	70	2.5	4.3	3
39	1000	70	2.3	4.3	3
40	1300	70	2.4	4.3	3
41	1600	70	2.3	4.3	3
42	1900	70	2.4	4.2	3
43	100	80	2.5	6.3	3
44	400	80	2.6	4.1	3
45	700	80	2.4	4.2	3
46	1000	80	2.5	4.2	3
47	1300	80	2.5	4.2	3
48	1600	80	2.2	4.1	3
49	1900	80	2.2	4.1	3

TABLE B.3

THE NINE ROUNDS OF EXPERIMENTS VARYING U_a, f, AND Q TO MAXIMIZE SEI IN PHASE 2.

Round	Exp.	Q (sccm)	U_a (kV)	f (kHz)	P (W)	SEI (eV atom^{-1})	δ_{SEI} (%)
0	1	500	5	30	1.120	0.031	4
	2	1000	4	20	0.509	0.007	4
	3	1500	4	20	0.586	0.005	4
	4	500	4	60	1.073	0.030	4
	5	1000	3	40	0.408	0.006	4
	6	2000	3	30	0.301	0.002	4
	7	500	4	20	0.516	0.014	4
	8	500	5	40	1.172	0.033	4
	9	1500	5	40	5.984	0.056	4
1	10	800	3.5	70	0.934	0.016	4
	11	2000	4	70	1.692	0.012	4
	12	800	4.5	55	1.416	0.025	4
	13	2000	5	35	1.467	0.010	4
	14	1600	5.5	40	2.184	0.019	4
2	15	1300	3.5	70	1.119	0.012	4
	16	1400	4.5	40	1.163	0.012	4
	17	1300	5	40	1.424	0.015	4
	18	1400	5.5	40	2.598	0.026	4
	19	1000	6	35	2.681	0.037	4
3	20	1700	4.5	50	2.796	0.023	4

Continued on next page

TABLE B.3 (CONTINUED)

Round	Exp.	Q (sccm)	U_a (kV)	f (kHz)	P (W)	SEI (eV atom^{-1})	δ_{SEI} (%)
	21	1600	5	40	5.689	0.050	4
	22	800	5.5	45	1.650	0.029	4
	23	2000	6.5	35	0.000	0.000	4
	24	2000	7	35	0.000	0.000	4
4	25	800	4	70	1.289	0.022	4
	26	2000	4.5	35	1.074	0.007	4
	27	1500	5	50	1.778	0.017	4
	28	900	5.5	40	1.687	0.026	4
	29	800	6	40	1.613	0.028	4

TABLE B.4

THE FIVE ROUNDS OF EXPERIMENTS ON ALL SEVEN DECISION VARIABLES TO MAXIMIZE σ AND MINIMIZE $T_{\max}$.

Round	Exp.	n	t_{on} (min)	t_{off} (min)	Q (sccm)	U_a (kV)	f (kHz)	d (mm)	P (W)	SEI (eV atom^{-1})	σ (S m^{-1})	T_{avg} (°C)	$T_{\max}$ (°C)	t_{active} (min)	t_{total} (min)
0	1	2	8.0	8.0	500	5	30	2.5	1.120	0.031	1.452	27.5	32.0	16	32
0	2	1	6.0	6.0	1000	4	20	4.5	0.509	0.007	1.477	24.3	26.2	6	12
0	3	3	7.0	7.0	1500	4	20	3.5	0.586	0.005	0.893	24.5	27.3	21	42
0	4	1	16.0	16.0	500	4	60	3.5	1.073	0.030	1.510	23.1	23.8	16	32
0	5	2	10.0	10.0	1000	3	40	2.5	0.408	0.006	1.222	25.5	28.4	20	40
0	6	3	9.0	9.0	2000	3	30	3.5	0.301	0.002	1.222	23.7	25.6	27	54
0	7	2	9.0	9.0	500	4	20	4.5	0.516	0.014	1.546	24.7	27.1	18	36
0	8	4	6.0	6.0	500	5	40	3.5	1.172	0.033	1.144	30.2	36.7	24	48
0	9	4	7.0	7.0	1500	5	40	4.5	5.984	0.056	3.650	49.1	77.5	28	56
1	10	4	7.0	7.0	800	6.5	45	4.5	7.611	0.132	6.850	60.1	73.5	28	56
2	11	50	0.5	0.8	800	6.5	45	4	7.611	0.132	6.311	39.8	48.6	25	63
2	12	50	0.7	1.0	800	6.5	45	4	7.611	0.132	6.549	52.7	58.7	33	83
4	23	36	0.5	1.2	800	6.5	45	2.5	7.611	0.132	7.272	42.7	46.5	18	60
4	25	24	0.5	2.0	800	6.5	45	2.5	7.611	0.132	4.310	39.2	43.9	12	60

B.5 Data-driven determination of experimental bounds for plasma jet operation (Phase 1)

Figures B.3 show parity plots for U_{on} (Figure B.3a) and U_{max} (Figure B.3b) based on the leave-one-out GPR predictions, where the dashed red line shows perfect correlation. For U_{on}, the leave-one-out root mean absolute error is 0.11 kV, which corresponds to relative errors $\leq$ 5.0% of the experimental values. For U_{max}, the leave-one-out root mean absolute error is 0.34 kV, which corresponds to relative errors $\leq$ 8.3% of the experimental values.

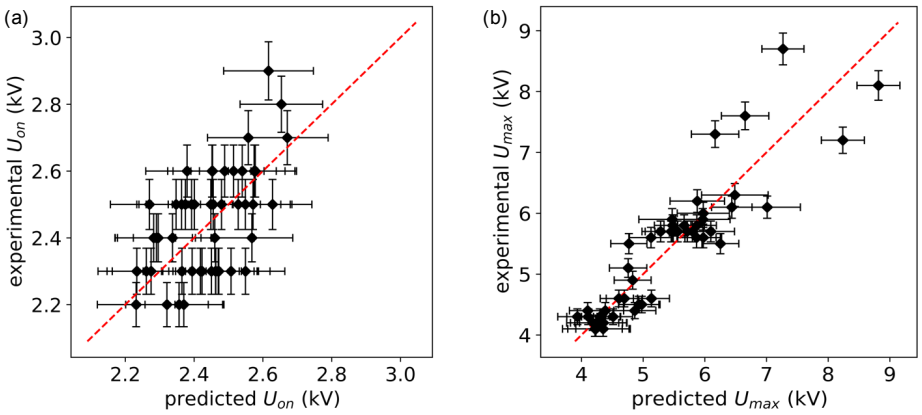

Figure B.3. Parity plots for leave-one-out predictions based on GPR models: (a) leave-one-out prediction of onset voltage (U_{on}); (b) leave-one-out prediction of maximum voltage (U_{max}). The experimental uncertainty for U_{on} and U_{max} is 3%. The dashed red line indicates perfect correlation.

B.6 Bayesian optimization of SEI (Phase 2)

Figures B.4 to B.13 illustrate detailed two-dimensional sensitivity analyses for different decision variables. The experiments of round 0, as shown in Fig. B.4, were conducted based on Latin hypercube sampling (LHS) recommendations. Since applied voltage (U_a) is one of the most influential factors for SEI, we discretized U_a into eight segments with 0.5 kV intervals and chose the jet flow rate (Q) and input frequency (f) based on (constrained) expected improvements for the following rounds.

In rounds 1 and 2, as shown in Fig. B.5 and Fig. B.6, respectively, we conducted experiments under five optimal experimental conditions for each round within the range of applied voltage from 3.5 to 6.0 kV. We noticed no improvement in SEI compared with the highest SEI obtained in round 0. Then, for round 3, shown in Fig. B.7, we considered high-voltage settings. We tried higher applied voltages, greater than 6.5 kV, and found that the plasma jet transitioned into an attached streamer on the substrate, damaging it. Hence, we implemented constraints to avoid these experimental conditions in our optimization process.

In round 4, shown in Fig. B.8, we followed the success of the constrained optimization and conducted experiments based on constrained expected improvement (CEI) recommendations. However, we did not observe any significant improvement in SEI and explored experiments recommended by expected improvement (EI). Therefore, in round 5, we considered experimental conditions recommended by both CEI and EI, as shown in Fig. B.9 and Fig. B.10, respectively.

In round 6, shown in Fig. B.11, we considered only EI recommendations, and we obtained a 62.5% improvement in the highest SEI compared with that in round 0. In rounds 7 and 8, shown in Fig. B.12 and Fig. B.13, respectively, we obtained higher SEIs compared with what we obtained in round 6. Our highest SEI (0.132 eV atom^{-1}) was obtained in round 8, a 136% improvement compared to round 0 (0.056

eV atom^{-1}). In summary, BO increased SEI by 2.4× compared with that before optimization.

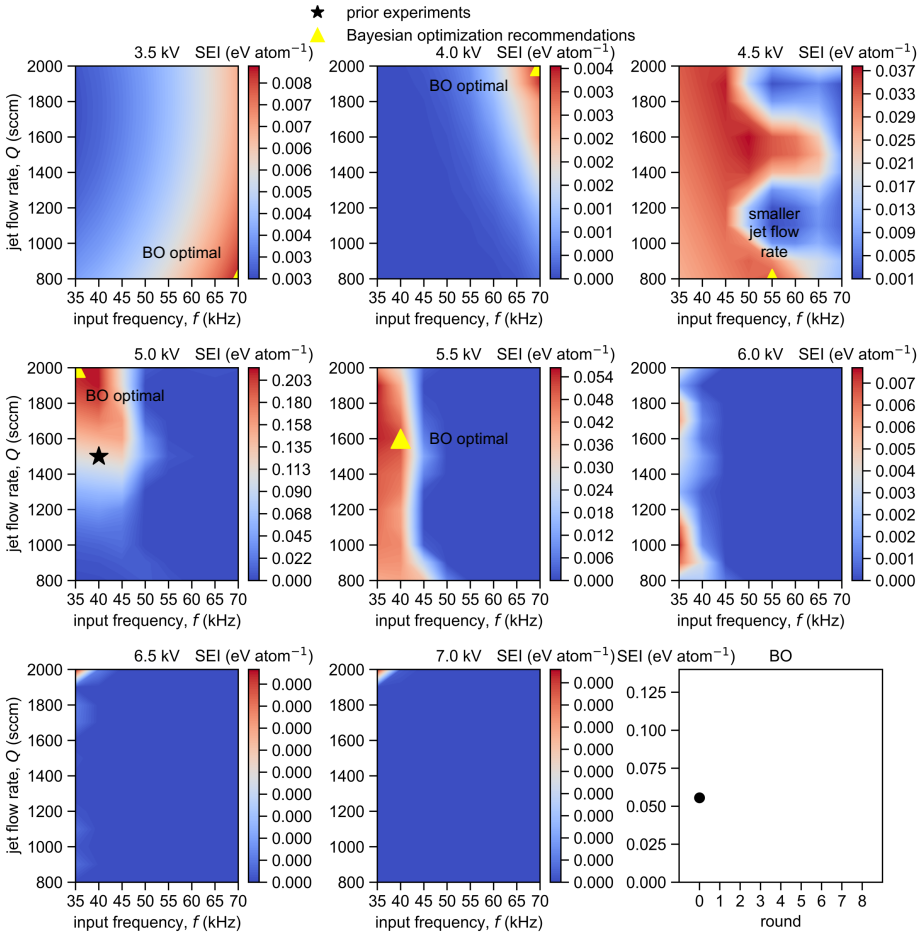

Figure B.4. Two-dimensional sensitivity analyses of constrained expected improvement (CEI) in round 0. The black stars are existing experimental data, and the yellow triangles are BO-recommended data.

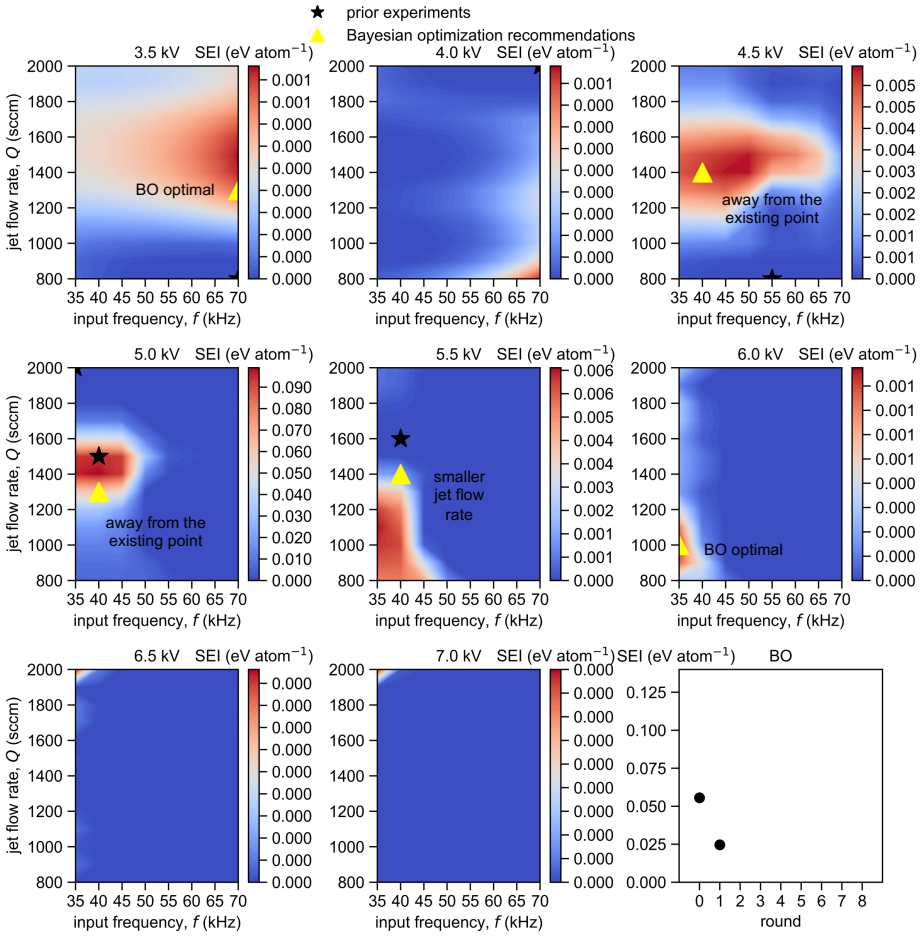

Figure B.5. Two-dimensional sensitivity analyses of constrained expected improvement (CEI) in round 1. The black stars are existing experimental data, and the yellow triangles are BO-recommended data.

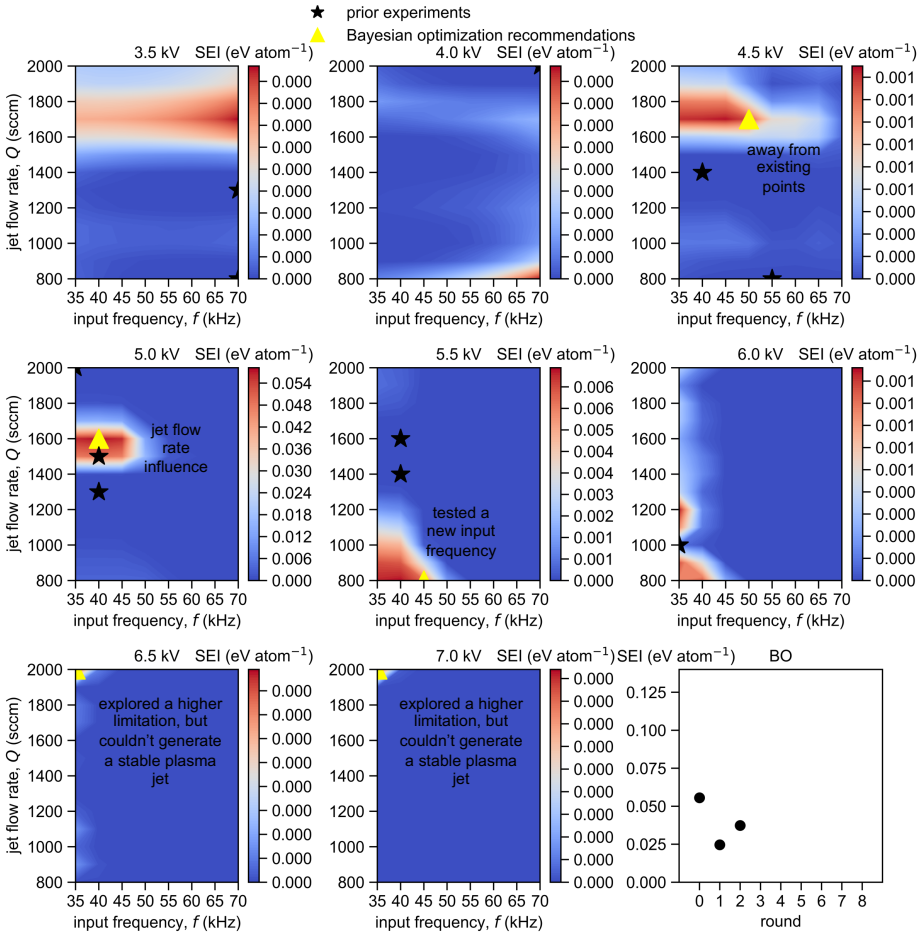

Figure B.6. Two-dimensional sensitivity analyses of constrained expected improvement (CEI) in round 2. The black stars are existing experimental data, and the yellow triangles are BO-recommended data.

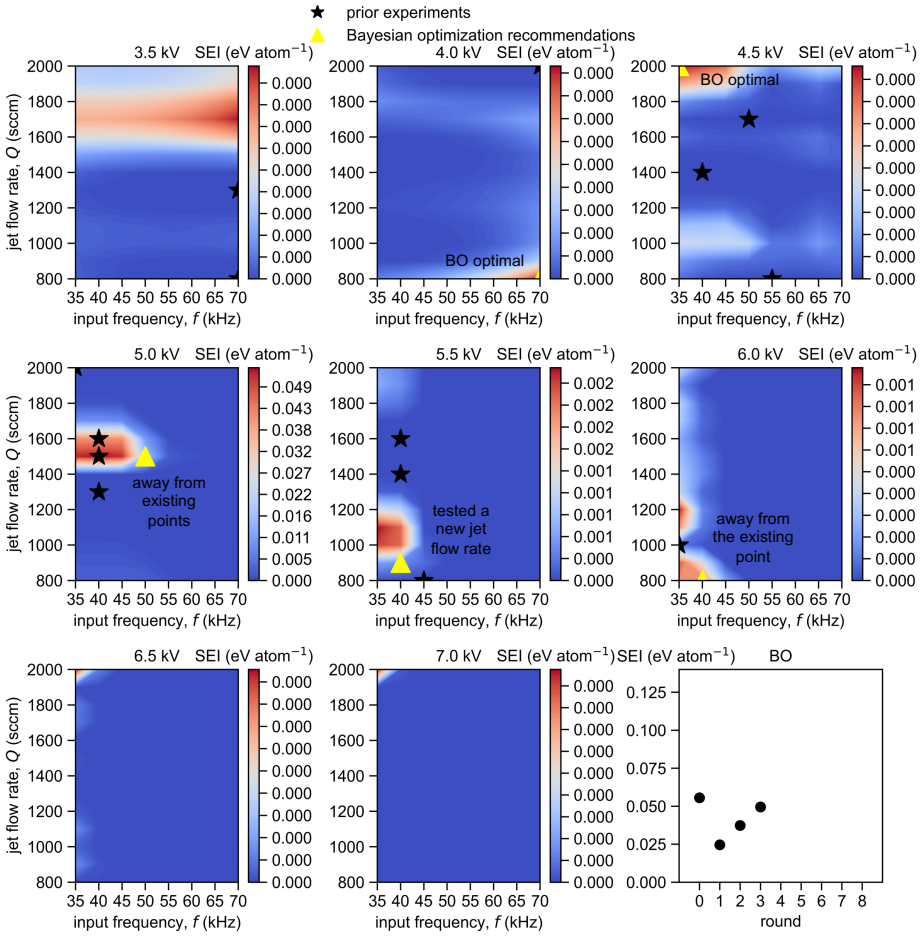

Figure B.7. Two-dimensional sensitivity analyses of constrained expected improvement (CEI) in round 3. The black stars are existing experimental data, and the yellow triangles are BO-recommended data.

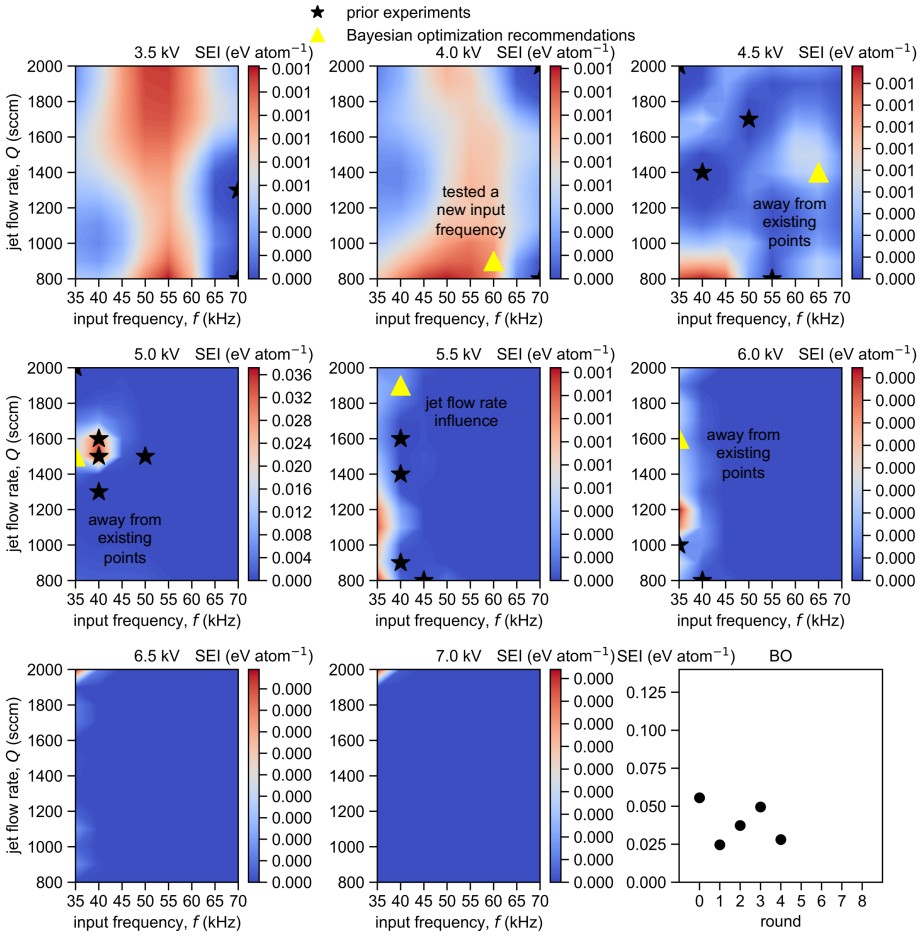

Figure B.8. Two-dimensional sensitivity analyses of constrained expected improvement (CEI) in round 4. The black stars are existing experimental data, and the yellow triangles are BO-recommended data.

B.7 Bayesian optimization for maximizing ITO film's electrical conductivity and minimizing substrate temperature (Phase 3)

B.7.1 Bayesian optimization for maximizing ITO film's electrical conductivity (Phase 3a)

Figures B.15 and B.16 illustrate two-dimensional sensitivity analyses for rounds 2 and 3, respectively.

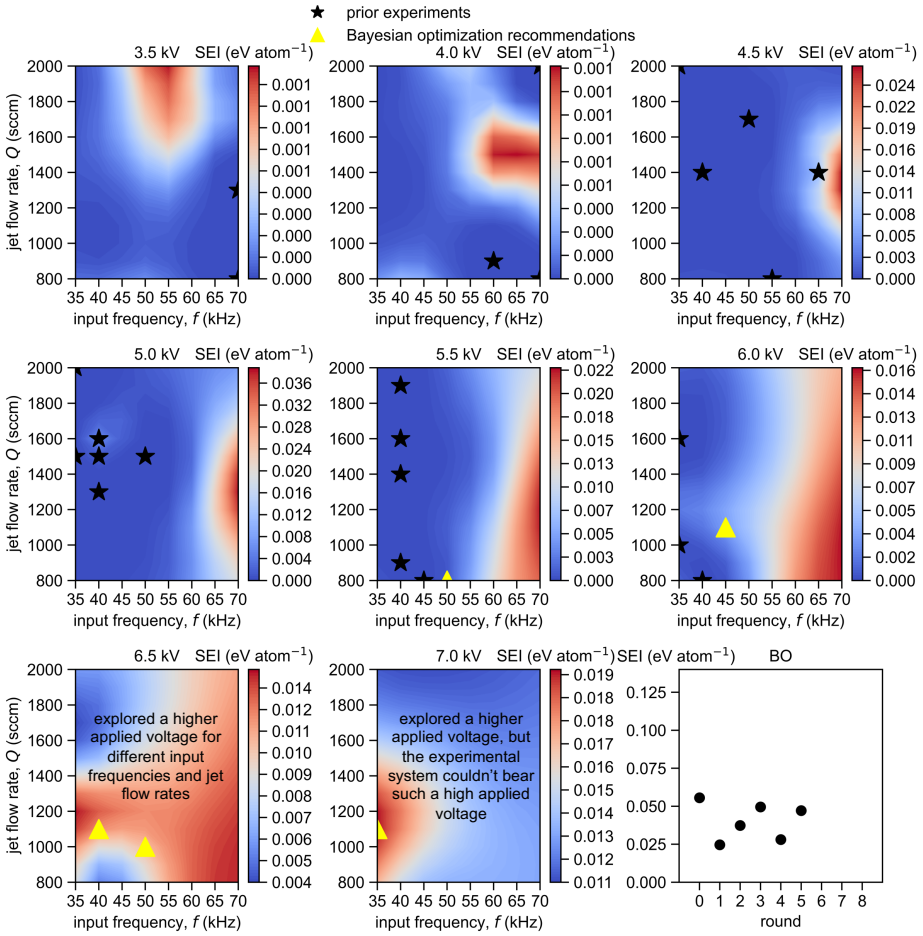

Figure B.9. Two-dimensional sensitivity analyses of expected improvement (EI) in round 5. The black stars are existing experimental data, and the yellow triangles are BO-recommended data.

Round 0: The initial round of nine plasma jet sintering experimental conditions was generated based on Latin hypercube sampling (LHS) recommendations.

Round 1: We conducted a single experiment using the jet flow rate (Q = 800 sccm), applied voltage (U_a = 6.5 kV), and input frequency (f = 45 kHz) values that produced the highest SEI in Phase 2 and the values for the other four decision variables (d = 4.5 mm, n = 4, t_{on} = 7 min, t_{off} = 7 min) from the experiment

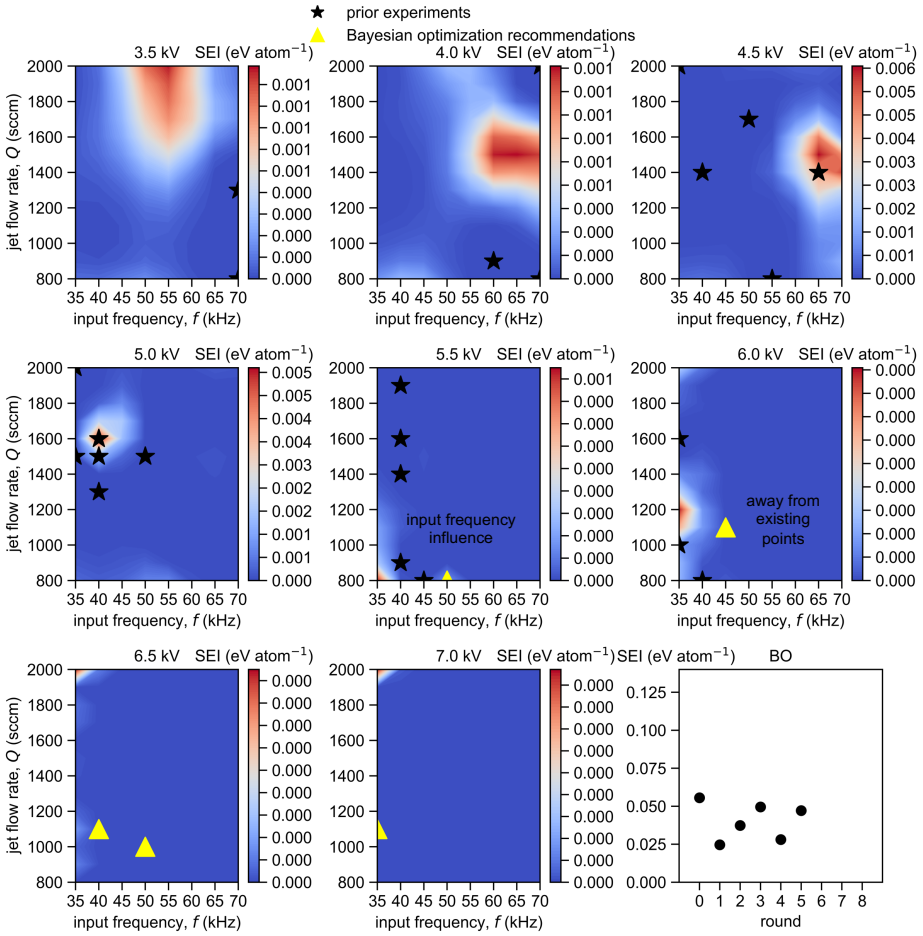

Figure B.10. Two-dimensional sensitivity analyses of constrained expected improvement (CEI) in round 5. The black stars are existing experimental data, and the yellow triangles are BO-recommended data.

that produced the largest electrical conductivity in round 0. We obtained an 87.7% improvement in electrical conductivity from 3.65 S m^{-1} to 6.85 S m^{-1}.

Round 2: The plasma jet sintering experimental conditions in round 2 were recommended by expected improvement (EI) between exploitation and exploration. Compared with the electrical conductivity we obtained in round 1, we achieved a 5% increase from 6.85 S m^{-1} to 7.191 S m^{-1} in round 2.

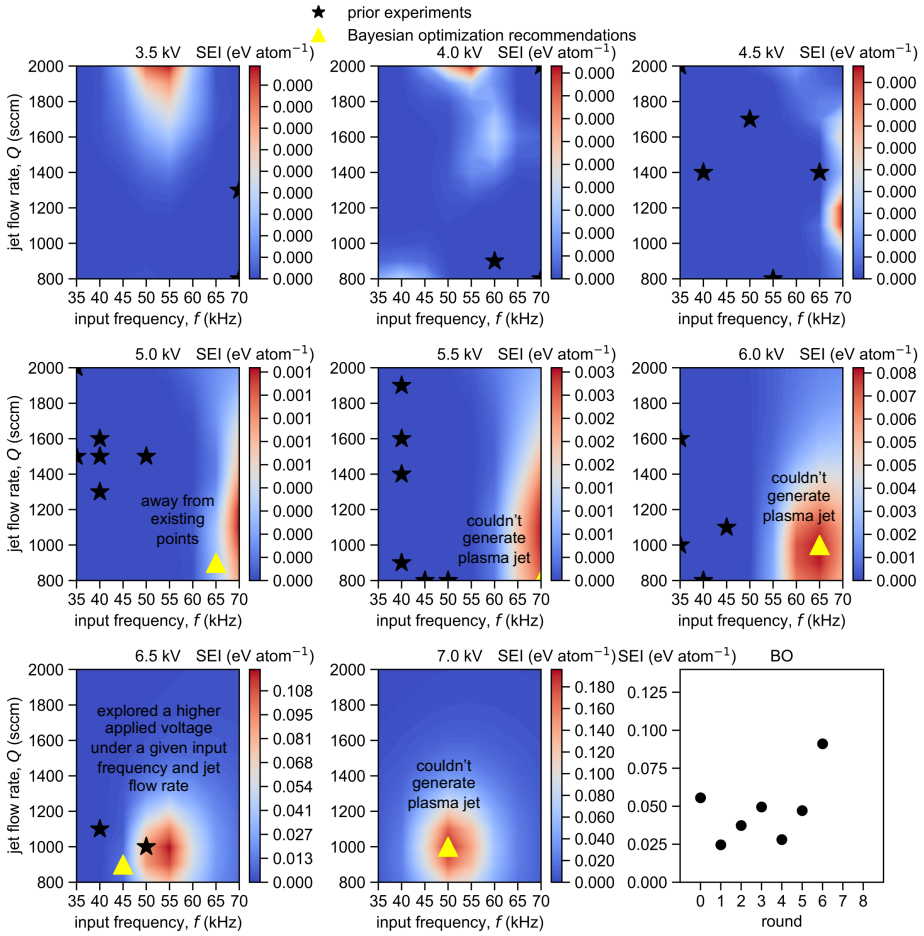

Figure B.11. Two-dimensional sensitivity analyses of expected improvement (EI) in round 6. The black stars are existing experimental data, and the yellow triangles are BO-recommended data.

Round 3: The plasma jet sintering experimental conditions in round 3 were recommended by expected improvement (EI) to explore decreasing d from 4.5 mm. Compared with the highest electrical conductivity we obtained in round 2, we achieved a 3% increase from 7.191 S m^{-1} to 7.421 S m^{-1} in round 3. However, the total experimental time of the highest-electrical conductivity experiment in round 3 was 125 minutes, and the peak substrate temperature reached 70.1 °C, which was greater than

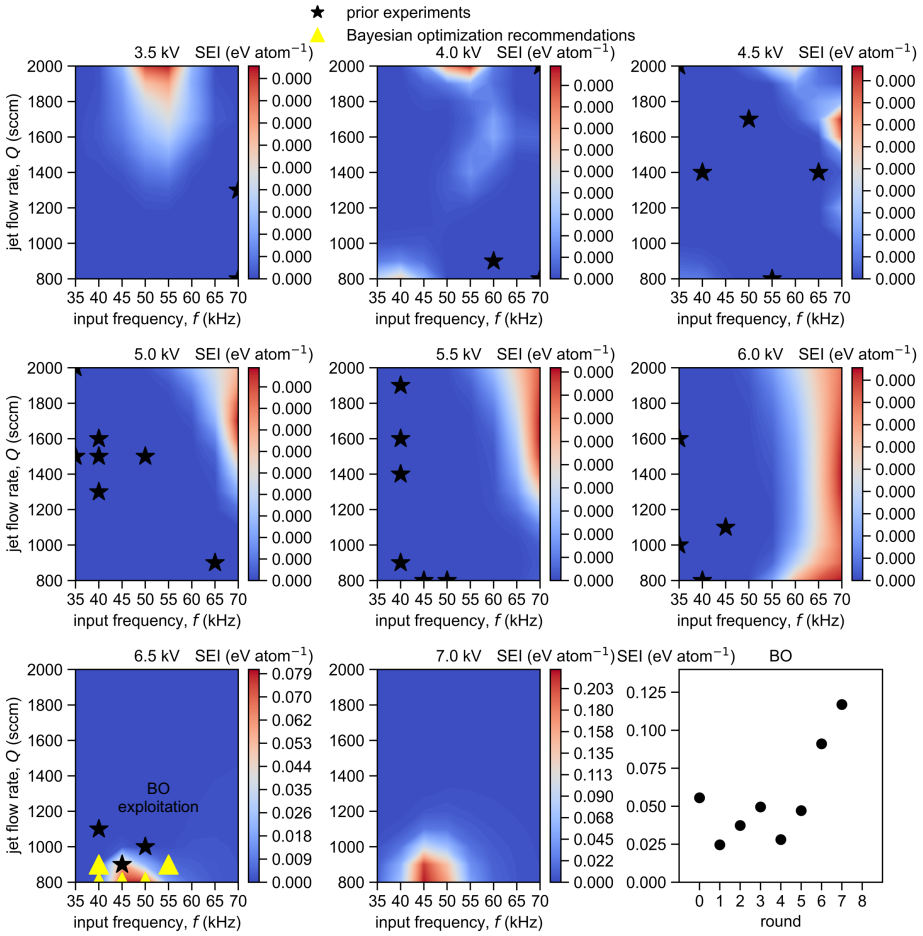

Figure B.12. Two-dimensional sensitivity analyses of expected improvement (EI) in round 7. The black stars are existing experimental data, and the yellow triangles are BO-recommended data.

the objective of controlling the substrate temperature below 50 °C.

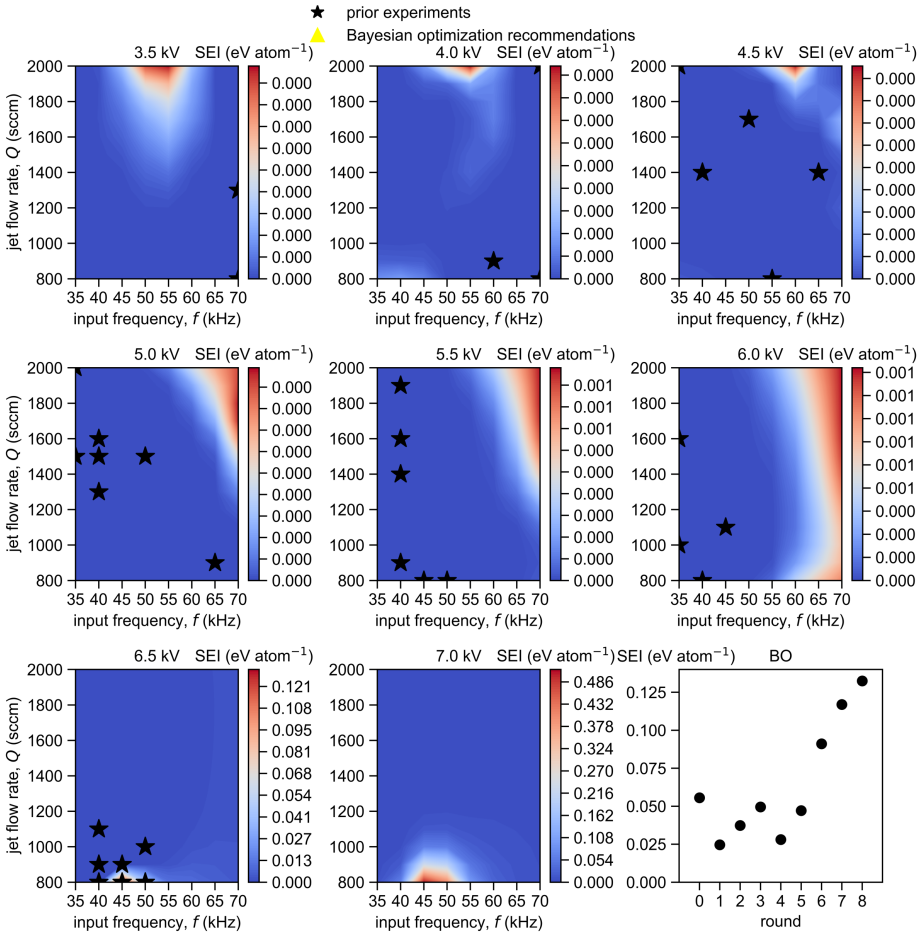

Figure B.13. Two-dimensional sensitivity analyses of expected improvement (EI) in round 8. The black stars are existing experimental data, and the yellow triangles are BO-recommended data.

B.7.2 Multi-objective optimization for maximizing ITO film's electrical conductivity while minimizing peak substrate temperature (Phase 3b)

Figures B.17a and B.17b illustrate the sensitivity analyses of the GPR prediction mean for electrical conductivity and peak substrate temperature, respectively, under the fixed jet flow rate (Q = 800 sccm), applied voltage (U_a = 6.5 kV), and input frequency (f = 45 kHz) values that produced the highest SEI (0.132 eV atom^{-1}).

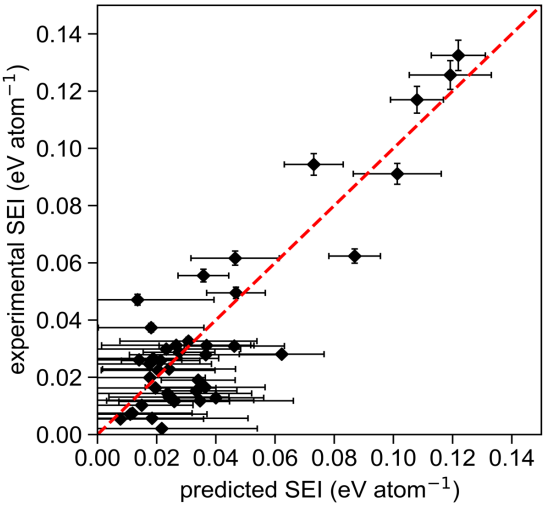

Figure B.14. Parity plot for leave-one-out prediction for SEI. The leave-one-out root mean absolute error is 0.03 eV atom^{-1} or 22.7% of the maximum obtained SEI. The dashed red line represents perfect correlation.

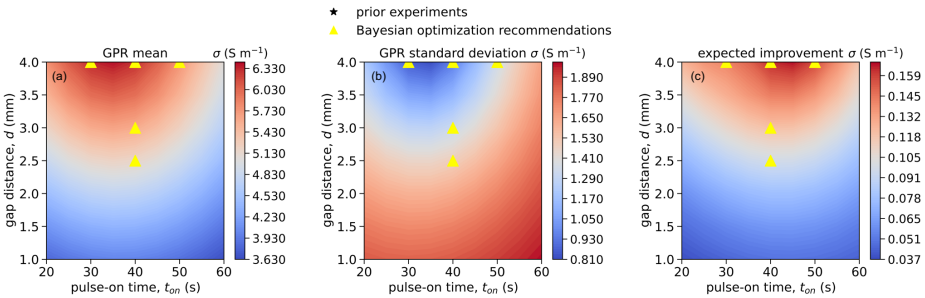

Figure B.15. Two-dimensional sensitivity analyses for round 2 show the GPR mean (left), standard deviation (middle), and expected improvement (right) predicted by BO. The yellow triangles are BO-recommended data.

Figure B.17a shows the two-dimensional sensitivity analyses for round 4, and Fig. B.17b shows the two-dimensional sensitivity analyses for round 5.

Round 4: In this round, we conducted sensitivity analyses on the influence of

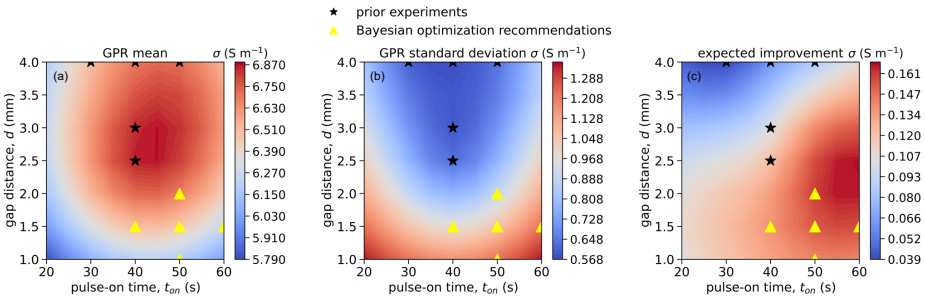

Figure B.16. Two-dimensional sensitivity analyses for round 3 show the GPR mean (left), standard deviation (middle), and expected improvement (right) predicted by BO. The black stars are existing experimental data, and the yellow triangles are BO-recommended data.

gap distance (d) and active sintering time (t_{active}) on improvements in the electrical conductivity of ITO films, as shown in Fig. B.17a. We also analyzed the influence of pulse-on time (t_{on}) and pulse-off time (t_{off}) on peak substrate temperature, as shown in Fig. B.17b. We found that if we fixed the jet flow rate (Q = 800 sccm), applied voltage (U_a = 6.5 kV), and input frequency (f = 45 kHz) values that produced the highest SEI (0.132 eV atom^{-1}), a 30-second pulse-on time (t_{on}) with a suitable number of cycles (n) was a good choice for controlling the peak substrate temperature below 50 °C.

As Fig. B.17a shows, the largest expected improvement is recommended at a gap distance of approximately 2.5 mm. Hence, we fixed the pulse-on time to 30 seconds and the gap distance to 2.5 mm. Then, we focused on another important factor, the total experimental time ($t_{\text{total}} = (t_{\text{on}} + t_{\text{off}}) \times n$) for one plasma jet sintering experiment. We conducted the experiments in round 4 with various numbers of cycles (n) and pulse-off times (t_{off}) but fixed the total experimental time to one hour. The recommended values of the number of cycles are shown in Fig. B.18a.

Round 5: We formulated our optimization problem as a multi-objective optimization and applied GPR models by considering enhancing the electrical conduc-

tivity and minimizing the peak substrate temperature simultaneously. For the experiments conducted in round 5, we tested two different total experimental times, 60 minutes and 30 minutes, aiming to determine if it was possible to obtain a lower peak substrate temperature while still achieving relatively high electrical conductivity in only 30 minutes.

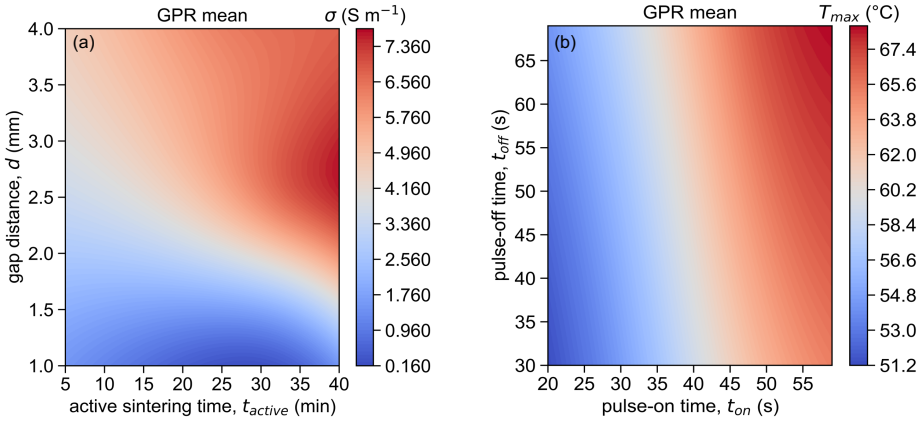

Figure B.17. (a) Sensitivity analysis of GPR prediction mean of sintered ITO films' electrical conductivity under fixed jet flow rate ($Q = 800$ sccm), applied voltage ($U_a = 6.5$ kV), and input frequency ($f = 45$ kHz) values that produced the highest SEI (0.132 eV atom^{-1}). The largest expected improvement region is located around a gap distance of 2.5 mm. (b) Sensitivity analysis of GPR prediction mean of peak substrate temperature under fixed jet flow rate ($Q = 800$ sccm), applied voltage ($U_a = 6.5$ kV), and input frequency ($f = 45$ kHz) values that produced the highest SEI (0.132 eV atom^{-1}).

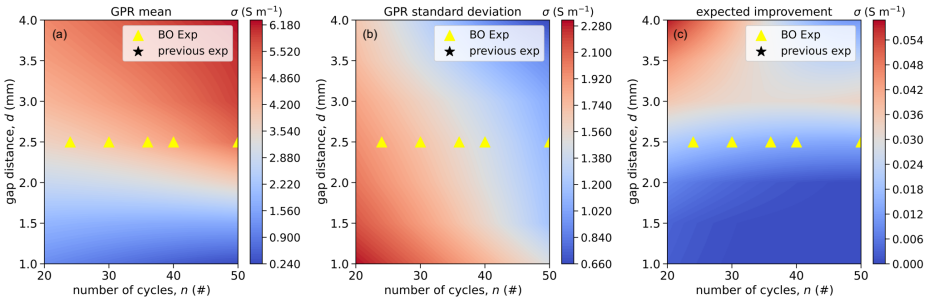

Figure B.18. BO of round 4 with two-dimensional sensitivity analyses for obtaining the largest electrical conductivity of ITO thin films. The two-dimensional sensitivity analyses illustrate GPR (a) mean, (b) standard deviation, and (c) expected improvement of BO. The black stars are existing experimental data, and the yellow triangles are BO-recommended data.

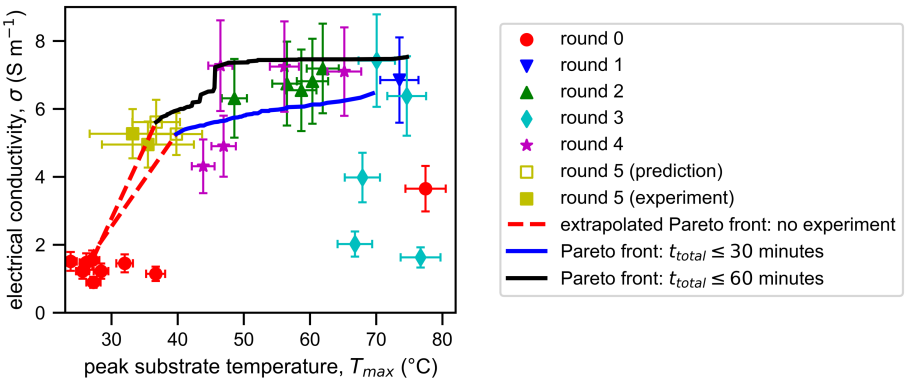

Figure B.19. Optimization of round 5 with Pareto set for obtaining the largest electrical conductivity of ITO thin films. The open yellow squares are the proposed experiments in round 5, and the filled yellow squares are the experimental results in round 5. The blue dashed curve shows the Pareto set based on a total experiment time (t_{total}) of 30 minutes. The black dashed curve shows the Pareto set based on a total experiment time (t_{total}) of 60 minutes. The red dashed curves show the extrapolated Pareto sets where there is no experimental data.

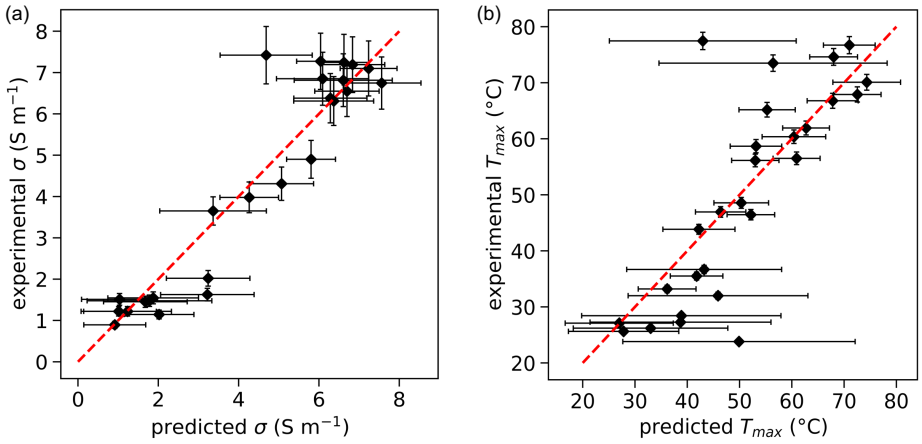

Figure B.20. (a) Parity plot of leave-one-out prediction of electrical conductivity. The leave-one-out root mean absolute error is 2.7 S m-1. (b) Parity plot of leave-one-out prediction of peak substrate temperature. The leave-one-out root mean absolute error is 18.4 °C.